NIH Public Access
Author Manuscript
Nucl Med Biol. Author manuscript; available in PMC 2014 January 01.

Published in final edited form as:
Nucl Med Biol. 2013 January ; 40(1): 3–14. doi:10.1016/j.nucmedbio.2012.08.004.

PET Imaging with ^{89}Zr: From Radiochemistry to the Clinic

Melissa A. Deri[1,2,*], **Brian M. Zeglis**[1,*], **Lynn C. Francesconi**[2], and **Jason S. Lewis**[1]

[1]Department of Radiology and the Program in Molecular Pharmacology and Chemistry, Memorial Sloan-Kettering Cancer Center, New York, NY, USA

[2]Department of Chemistry, Hunter College and the Graduate Center of the City University of New York, New York, NY, USA.

Abstract

The advent of antibody-based cancer therapeutics has led to the concomitant rise in the development of companion diagnostics for these therapies, particularly nuclear imaging agents. A number of radioisotopes have been employed for antibody-based PET and SPECT imaging, notably ^{64}Cu, ^{124}I, ^{111}In, and ^{99m}Tc; in recent years, however, the field has increasingly focused on ^{89}Zr, a radiometal with near ideal physical and chemical properties for immunoPET imaging. In the review at hand, we seek to provide a comprehensive portrait of the current state of ^{89}Zr radiochemical and imaging research, including work into the production and purification of the isotope, the synthesis of new chelators, the development of new bioconjugation strategies, the creation of novel ^{89}Zr-based agents for preclinical imaging studies, and the translation of ^{89}Zr-labeled radiopharmaceuticals to the clinic. Particular attention will also be dedicated to emerging trends in the field, ^{89}Zr-based imaging applications using vectors other than antibodies, the comparative advantages and limitations of ^{89}Zr-based imaging compared to that with other isotopes, and areas that would benefit from more extensive investigation. At bottom, it is hoped that this review will provide both the experienced investigator and new scientist with a full and critical overview of this exciting and fast-developing field.

Keywords

PET Imaging; ImmunoPET; Radiochemistry; Antibody; ^{89}Zr

Introduction

The exquisite specificity and affinity of antibodies have made them extremely attractive candidates for cancer therapeutics and drug delivery agents. Consequently, over the past two decades, considerable effort has been invested into the construction and development of antibody-based imaging agents as companion diagnostics for the characterization, treatment planning, and treatment monitoring of cancer. Importantly, one of the most fundamental principles in the construction of effective antibody-based nuclear imaging agents is matching the physical half-life of the radioisotope to the pharmacokinetic half-life of the

Corresponding Author: Jason S. Lewis; Sloan-Kettering Institute, 1275 York Avenue, New York, NY 10065; Phone, 646-888-3039; Fax, 646-888-3059; lewisj2@mskcc.org.
*These authors contributed equally to the preparation of this manuscript

immunoglobulin.[3] Generally, intact antibodies have relatively slow pharmacokinetics, often requiring multiple days to reach their optimal biodistribution within the body. As a result, up until just a few years ago, the exigency of matching physical and biological half-lives has led ^{111}In, ^{99m}Tc, ^{67}Ga, ^{86}Y, ^{64}Cu, and ^{124}I — with half-lives of 2.80 d, 6.0 h, 3.26 d, 14.74 h, 12.70 h, and 4.18 d, respectively — to be the most often employed radioisotopes for antibody-based nuclear imaging agents.[4]

Each of these isotopes, however, possesses characteristics that ultimately limit their suitability for clinical antibody-based imaging. ^{64}Cu, for example, has been employed successfully as a radiolabel for antibodies in numerous pre-clinical studies in rodents, but its 12.7 h half-life is ultimately too short to prove effective under the slower pharmacokinetic conditions of imaging in humans.[5-8] ^{86}Y likewise possesses a half-life that is too short for human imaging and also adds the limitations of sub-optimal decay characteristics and difficult radionuclide production and purification protocols. ^{124}I, in contrast, has a near ideal half-life for antibody-based imaging and has thus long been the radionuclide of choice for immunoPET.[9, 10] However, the expense of the isotope, its relatively low resolution due to the high energy of its positrons, and the significant dehalogenation of ^{124}I-labeled antibodies *in vivo* combine to limit its ultimate clinical potential. Finally, while ^{111}In and ^{67}Ga also boast favorable physical half-lives and behavior for antibody-based applications, the inherent limitations of SPECT relative to its higher resolution and quantitative cousin, PET, have resulted in a far greater interest in the clinical translation of immunoPET agents rather than radiopharmaceuticals for immunoSPECT. ^{99m}Tc, of course, combines the aforementioned limitations of SPECT imaging with a half-life that is regarded as too short for clinical antibody-based imaging.

The desire to find a more suitable radioisotope for antibody-based imaging has been the driving force behind the recent increase in research into ^{89}Zr-based imaging, led by the laboratories of Elisabeth de Vries and Guus van Dongen in the Netherlands, among others.[11-14] Indeed, ^{89}Zr has favorable physical characteristics for antibody-based imaging, with a half-life of 78.4 h and a relatively low positron energy of 395.5 keV, and its advantages over the alternatives are manifold: its physical half-life is better suited to antibody-based imaging than that of ^{64}Cu or ^{86}Y, particularly in the clinic; it is safer to handle, cheaper to produce, more stable *in vivo*, and residualizes in tumors far more effectively than ^{124}I; additionally, its emission of positrons rather than single photons allows for higher resolution, quantitative imaging.[15, 16] Taken together, these characteristics have spurred the rise of ^{89}Zr from a relatively obscure positron-emitting radiometal less than ten years ago to a popular choice for both pre-clinical and clinical immunoPET imaging. To wit, prior to 2009, the number of publications per year on ^{89}Zr-PET hovered between 2-6; in 2009, however, this number rose 10, followed by even more pronounced increases to 27 and 33 in 2010 and 2011, respectively. Finally, it is also important to note that while antibodies represent perhaps the most significant and promising application of ^{89}Zr, the isotope may also prove useful with other types of targeting vectors, particularly nanoparticles with slow pharmacokinetics and peptides for which longer imaging studies may prove informative.

In the following pages, we hope to provide a comprehensive review of the rapidly growing field of ^{89}Zr-based PET imaging. It would be remiss not to mention that other excellent reviews on ^{89}Zr currently exist in the literature, especially those written by Vugts and van Dongen at Vrije University in the Netherlands and Severin and Nickles at the University of Wisconsin. [17, 18] Our more comprehensive review stands apart from these, however, as the former focuses primarily on ^{89}Zr radiochemistry, and the latter primarily addresses conjugation methodologies; others that have recently appeared in the literature have concentrated on ^{89}Zr production[19] or its use in pre-clinical imaging[20] or have discussed ^{89}Zr in a broader context of PET radiometals or developing radiopharmaceuticals.

[4, 21-23] In contrast, in the following pages, we will strive to cover a wide range of topics, ranging from ^{89}Zr production and purification to the design and bioconjugation of chelators for ^{89}Zr to the most recent clinical imaging studies. Ultimately, it is our hope that this review will provide a comprehensive and in-depth portrait of the current state of the field, illustrate both the successes and limitations of ^{89}Zr-based imaging, help identify specific areas that are in need of additional research, and, in so doing, prove useful to the scientist new to the field and veteran investigator alike.

Decay Characteristics

Any discussion of PET imaging with ^{89}Zr must necessarily begin with the fundamentals its decay [24-28]. ^{89}Zr decays with a half-life of 78.41 h via both positron emission and electron capture to an intermediate ^{89m}Y state which in turn decays to stable ^{89}Y via a gamma ray emission (909 keV) with a half-life of 15.7 s (Figure 1). The relatively low translational energy of the emitted positrons, 395.5 keV, results in high image resolution, and the energy disparity between the 511 keV photons and the 909 keV gamma rays prevents the latter from interfering with the detection of the coincident photons. Importantly, the suitability of the ^{89}Zr decay characteristics for imaging markedly contrasts with ^{124}I, which emits much higher energy positrons (687 and 974 keV) and also emits a number of photons with energies within 100-150 keV of the positron-created 511 keV [27]. Both phenomena combine to grant ^{89}Zr noticeably better resolution than its halogen competitor.

Despite its favorable physical properties overall, an important practical consideration with ^{89}Zr is its abundant 909 keV gamma-ray; this high-energy, highly penetrating photon is emitted in 99% of ^{89}Zr decays. The half-value layer in lead for 909 keV photons is ~10 mm, about that twice that for 511-keV photons. ^{89}Zr will thus necessitate more shielding for transport and safe handling than is generally considered adequate for pure positron emitters such as ^{18}F.

Production and Purification

^{89}Zr has been produced on a cyclotron via both the ^{89}Y(*p,n*)^{89}Zr and ^{89}Y(*d,2n*)^{89}Zr reactions.[18, 25, 26, 29-31] In both cases, these routes provide the added advantage of employing a ^{89}Y metal target that is commercially available, non-reactive, and in 100% natural abundance, which drives down costs and precludes the need for cumbersome recycling of the target. For the deuterium reaction, a minimum beam energy of 5.6 MeV is required.[31] In practice, the proton reaction is the much more popular of the two and typically employs proton beams at or above 14 MeV, though early reports employed beams of 13 MeV. In both cases, the avoidance of the isotopic impurity ^{88}Zr by inadvertent (p, 2n) or (d, 3n) reactions, respectively, poses a particular concern, for both ^{88}Zr ($t_{1/2}$ = 83.4 d) and its daughter ^{88}Y ($t_{1/2}$ = 106 d) are potentially complicating impurities.[30, 31]

The isolation and purification of ^{89}Zr have been subjects of considerable interest. Methods ranging from solvent extraction to anion exchange chromatography have been employed, though weak cation exchange chromatography using hydroxamate-modified resin has emerged as the method of choice [25, 29, 31-33]. Using this method, the ^{89}Zr is loaded onto a column of hydroxamate resin in 2 M HCl, washed with additional 2 M HCl and metal-free water, and eluted in a 1.0 M oxalic acid solution that can then be employed for radiolabeling reactions. As a practical example of the techniques for production and purification described above, at Memorial Sloan-Kettering Cancer Center in New York City, ^{89}Zr is produced via the ^{89}Y(*p,n*)^{89}Zr reaction using a ^{89}Y thin-foil target (99% purity, 0.1 mm width) using a 15 MeV proton beam and a 10° angle of incidence to the target. Using these conditions and the hydroxamate resin purification methodology described above, ^{89}Zr is produced reliably and

reproducibly in high specific activity (470–1195 mCi/mmol) and radionuclidic purity (>99.99%).[26]

Zirconium Chemistry

As we progress, a fundamental understanding of the aqueous chemistry of zirconium is critical, both to better evaluate the coordinative relationship between the zirconium cation and its chelator and to provide insight into the possible behavior of the metal if it were released from its chelate *in vivo*.

Basics

Zirconium is a group IV metal, which exists primarily as a +4 ion in aqueous solution. This Zr^{4+} cation is a relatively large, highly-charged ion which typically forms coordination complexes with high coordination numbers, and, as a 'hard' cation, typically prefers anionic oxygen donors.[34] The effective ionic radius of the Zr^{4+} cation with a coordination number of eight is 0.84 angstroms.[35] The complexity of aqueous zirconium chemistry has led to somewhat limited study of the area. Oxides and hydroxides of zirconium exhibit very poor solubility in water, less than 10^{-8} M, as well as pH-dependent changes in speciation. At very low pH, less than zero, zirconium forms polynuclear species upon hydrolysis, while under slightly less acidic conditions, between zero and two, mononuclear hydrolysis species predominate. However, around pH two, the solubility of the zirconium species decreases and precipitation can occur.[36] Even at very low pH, delicate equilibria exist between different polynuclear zirconium species and slight changes in pH can lead to aggregation.[37] In contrast to the zirconium hydroxide species, Zr^{4+} salts of halides, perchlorate, and sulfate are soluble in acidic solution. [34]

Outside of its radioisotopic applications that form the focus of this review, zirconium is heavily used in ceramics, some of which are used in medical prosthetic applications, in the form of zirconia or ZrO_2.[38] Additionally, due to the low neutron capture cross section of zirconium, its metal alloys are used for cladding in nuclear reactors. However, the predominant use of zirconium in chemistry is in the application of organometallic catalysis including olefin metathesis[39], ring-opening polymerizations[40], aminoalkene hydroamination[41], and other reactions.[42-44] For different catalytic and waste separation purposes, a number of different zirconium coordination complexes have been studied, however, in the context of the construction of ^{89}Zr-labeled bioconjugates for PET, only a handful of stable, aqueous, bio-compatible complexes are appropriate.

Chelation

The foundation of any biomolecular PET tracer lies in the formation of a stable radiometal chelate. To date, a number of different aqueous chelators have been employed with zirconium (Figure 2), of which desferrioxamine B (DFO) has become by far the most successful and oft-employed.

Prior to the development of any specialized ligands for Zr^{4+}, the majority of research into the coordination chemistry of Zr employed some of the most commonly used bifunctional chelates: ethylenediaminetetraacetic acid (EDTA), diethylenetriaminepentaacetic acid (DTPA), and 1,4,7,10-tetraazacyclododecane-1,4,7,10-tetraacetic acid (DOTA). Crystal structures have been obtained for Zr-EDTA [45] and Zr-DTPA[46], and a solution structure has been obtained in the case of Zr-DOTA using NMR methodologies [47]. Despite the differences in chelators, each structure indicates a coordination number of eight. EDTA binds zirconium through two nitrogen atoms, four oxygen atoms, and two exogenous water molecules, whereas both DTPA and DOTA coordinate the metal using solely the constituent atoms of the ligand: three nitrogens and five oxygens for DTPA and four of each atom for

DOTA. The log K values for thermodynamic stability constants are reported as 29.4 for Zr-EDTA at 25°C in water and an ionic strength of 0.1 and 35.8 for Zr-DTPA at 20°C in water and an ionic strength of 0.23, but remain unreported for Zr-DOTA.[48] The higher thermodynamic stability of Zr-DTPA is most likely due to the fact that DTPA coordinatively saturates the Zr^{4+}, in contrast to EDTA which requires two exogenous water molecules to complete the coordination sphere. Despite this, an attempt to radiolabel an antibody using DTPA as the chelator resulted in less than 0.1% successful labeling.[49]

A different tactic for finding chelators came from the study of siderophores or natural iron-chelating molecules produced by bacteria. The most prominent chelator of Zr^{4+} currently employed, desferrioxamine (DFO), is an example of a hexadentate, bifunctional siderophore with three hydroxamate groups for chelating metals and a primary amine tail which can be modified for conjugation to a biomolecule (Figure 3). Investigations in the 1960s involving the reprocessing of nuclear fuel found that zirconium had an affinity for hydroxamic acid groups, displaying stability constants of $\beta_1=2.7\times10^{12}$ and $\beta_2=1.2\times10^{24}$ with respect to benzohydroxamic acid.[50] It follows, then, that the presence of the hydroxamate groups in DFO would make it a suitable and effective chelator for Zr^{4+}, and indeed, the success of the vast majority of ^{89}Zr-based PET imaging is a testament to the value of DFO as a chelator. In one of the earliest investigations into the utility of ^{89}Zr as a PET radionuclide, Meijs and co-workers reported that DFO exhibits rapid and efficient labeling with a 1:1 ratio of metal to chelate and demonstrates good stability with regard to demetallation, releasing less than 0.2% of the metal in serum after 24 hours.[51] Further evaluation of the complex by Holland and coworkers utilizing density functional theory (DFT) models Zr-DFO as an octadentate complex combining the six binding oxygens of DFO with two additional water molecules. Also, stability studies over longer periods of time indicated that still less than 2% demetallation occurs after seven days in serum.[52] Unfortunately, thus far, neither physical structural studies nor thermodynamic stability constants have been reported for Zr-DFO.

While DFO is by far the most widely used zirconium chelator and behaves reasonably well *in vivo*, there is a growing school of thought that an even better ligand could be designed and synthesized. The most basic argument here is that zirconium favors octadentate coordination, and the DFO ligand itself only offers hexadentate chelation, leaving the bound ^{89}Zr exposed to solvent. As discussed above, DFT modeling of DFO and Zr^{4+} suggests that two water molecules are bound to the zirconium in addition to DFO, reinforcing this idea. A ligand that incorporates all eight binding sites for Zr^{4+} should benefit from the preorganization of the coordination environment and thus should demonstrate superior stability compared to DFO when complexed with ^{89}Zr. However, initial experiments with ligands such as EDTA, DTPA, and DOTA illustrated that these ligands, despite achieving higher coordination numbers, form complexes with lower stability compared to DFO. While not proven, the reduction in stability in these cases is likely due to the additional chelation arising from nitrogen atoms, rather than the oxygen donors preferred by the oxophilic Zr^{4+} cation. Ultimately, it is believed that the ideal solution for stable Zr^{4+} chelation would be a ligand that is both octadentate and oxygen-rich. More specifically, catechols, hydroxypyridinones, and hydroxamates are likely candidates for binding groups. Investigations are currently underway at a number of institutions toward the design, synthesis, and evaluation of novel, high-stability Zr^{4+} ligands. A more robust, stable ligand for ^{89}Zr would help minimize the release of free $^{89}Zr^{4+}$ *in vivo* and thus help alleviate the concern over dose to bone and other non-targeted organs.

Conjugation Chemistry

With the selection of a targeting vector and radiometal-chelate pair comes the necessity for a method to covalently link the units together. In the case of ^{89}Zr, the overwhelming majority

of bioconjugates have utilized DFO as the chelator, so that will be the focus of the following discussion. The conjugation of DFO to an antibody or other construct has been achieved in a variety of ways: exploiting thiol linkages, amide couplings, and even click chemistry (Figure 3). Taken together, these conjugation techniques are based most frequently on the reaction of an activated bifunctional chelator with a lysine or cysteine residue of the protein.

Early work

Some of the earliest work of attaching DFO to an antibody comes not from the zirconium literature, but rather from past work on ^{67}Ga-based radiopharmaceuticals. In these cases, conjugation was accomplished by modifying both the primary amine of a lysine residue on an antibody and the amine tail of DFO with hetero-bifunctional agents and then joining the units together. For example, the modification of each piece with *N*-succinimidyl-3-(2-pyridyldithio) propionate (SPDP) allows for the formation of a disulfide linkage and *N*-(6-maleimidocaproyloxy)succinimide (EMCS) can be used to attach a maleimide functionality to DFO which could then be connected to a thiolated antibody. Alternatively, a homo-bifunctional agent such as glutaraldehyde can be used to connect the antibody and chelate in one step. This method, however, comes with the risk of the antibody linking to itself and forming polymers instead of creating one to one antibody-chelate complexes.[53] With the advent of ^{89}Zr as a radionuclide for PET imaging came an increased interest in DFO-antibody conjugation. At this time, the utilization of hetero-bifunctional agents had evolved to using two different compounds, namely *N*-succinimidyl-*S*-acetylthioacetate (SATA) to append the antibody and succinimidyl 4-(*N*-maleimidomethyl)cyclohexane- 1 -carboxylate (SMCC) to modify DFO. These two structures could then be combined through the formation of a succinimide ring-thioether bond.[54] However, it was later shown that such a linkage was unstable at physiological pH.[55]

Lysine methods

A major breakthrough was made by Verel and coworkers with the introduction of a new conjugation method utilizing an activated 2,3,5,6-tetrafluorophenol (TFP) ester of DFO that could be coupled to the unmodified, native lysine side-chains of an antibody. This involves a five step procedure which includes the extension of DFO with succinyl anhydride, the protection of the ligand's hydroxamate groups with Fe(III), the formation of the activated TFP ester, conjugation to the unmodified antibody, and removal of the iron to free the chelate for radiolabeling.[33] Conjugation in this manner with Fe-coordinated TFP-*N*-succinylDFO (*N*-suc-DFO) offers a reliable procedure to form a stable linkage without the need to pre-modify the antibody with its own bifunctional moiety and has to date been the most prevalent conjugation method used in preclinical ^{89}Zr PET imaging. More recently, Perk and Vosjan *et al.* introduced an even simpler method using a *p*-isothiocyanatobenzyl-bearing DFO (DFO-Bz-NCS). This commercially available chelate can be attached to the lysine residues of an unmodified antibody in one step, forming a stable thiourea linkage between chelator and biomolecule.[56, 57] In only the few years that the isothiocyanate derivative has been available, it has gained popularity due to its simplicity. However, it is not a perfect solution, primarily due to the water insolubility of the *p*-isothiocyanatobenzyl-DFO precursor, which requires more finesse than the straightforward *N*-suc-DFO chemistry.

Thiol methods

A significant concern with regard to the lysine-based conjugation methodologies is that nonspecific attachment of a chelator to an antibody has the potential to hinder immunoreactivity by attaching the chelate at an antigen-binding site. In response to this problem, increasing attention has been dedicated to the development of site-specific conjugation strategies using engineered cysteine residues. In the most prevalent example of this approach, the thiol-reactive DFO derivatives bromoacetamido-desferrioxamine (DFO-

Bac), iodoacetamido-desferrioxamine (DFO-Iac), and maleimidocyclohexyl-desferrioxamine (DFO-Chx-Mal) were constructed and then attached to cysteine residues designed into non-bioactive sites on an antibody. Both DFO-Bac and DFO-Iac attach to the cysteine through nucleophilic substitution reactions, whereas DFO-Chx-Mal undergoes a Michael addition with the residue. The resulting radiolabeled antibodies were found to be stable and demonstrated imaging characteristics analogous to the lysine-linked complexes. In the models tested, however, no significant advantage in immunoreactivity was demonstrated for site-specific conjugation.[58]

Click methods

Very recently, the use of click chemistry has emerged as a specialized conjugation method to expand the scope of ^{89}Zr PET imaging possibilities. A click strategy using an inverse electron demand Diels-Alder reaction between the strained dienophile norbornene and 3-(4-benzylamino)-1,2,4,5-tetrazine has been harnessed by coupling a norbornene functionality to lysine residues of an antibody and attaching a tetrazine to DFO. The benefit of this type of click chemistry is that it allows for modularity, allowing researchers to switch out different chelator-radiometal pairs or different antibodies while still maintaining the same overall conjugation methodology.[59] Another click-based strategy attempted to take advantage of the Staudinger ligation between azides and phosphines for use in pre-targeting experiments by reacting azide-modified antibodies with phosphine-containing radiometal-chelate complexes such as ^{89}Zr-DFO-phosphine. Unfortunately however, the Staudinger ligation was found thus far to be incompatible *in vivo*.[60]

Choosing a Conjugation Strategy

With such a variety of methods, it becomes important to select a conjugation method that fits the task at hand. In most cases, the *N*-suc-DFO or DFO-Bz-NCS methods are more than adequate, and while the most commonly used conjugation method is currently the N-succinyl-DFO TFP ester, one would expect that the already increasing use of the p-isothiocyanate method will only become more widespread due to the fact that it is a more rapid and facile method and it employs commercially available starting materials. More specialized situations, however, may call for other routes. For example, the site specific system is particularly appropriate in cases where the loss of immunoreactivity is a concern, and the click methodology may prove beneficial where modularity is desired. As the field continues to expand and ^{89}Zr-based imaging moves further into the mainstream, it is hoped that new methodologies will be developed that may combine the convenience of a commercially available starting materials with some of the benefits of the other systems.

Zirconium Biochemistry

Moving from the test tube to the body, the behavior of free Zr^{4+} within biological systems has been studied in order to gauge the safety of using ^{89}Zr as a PET tracer as well as to better understand the fate of the radionuclide in the case of metabolism of parts of the radiopharmaceutical. This is especially important in the case of zirconium because of the high affinity of Zr^{4+} for bone.

Biodistribution

The normal composition of the human body includes small amounts of zirconium found in fat, liver, and gall bladder tissue, as well as trace amounts in the brain. Excretion of zirconium from food and water intake is thought to involve the hepatobiliary system and results in fecal, rather than urinary, excretion.[38] The fate of non-dietary zirconium, however, is less straightforward and depends upon the chemical speciation of the metal cation as well as perhaps the organism into which it is administered.

An example of the clearance mechanism and rate varying between species can be seen when Zr^{4+} is complexed by citrate. In rats, 80-90% of Zr-citrate is rapidly excreted in the urine within 24 hours[61], while in mice, only 30% of Zr-citrate was cleared within 24 hours.[62] In an early study of ^{89}Zr-citrate in man, activity was only found in the plasma of blood and zirconium was shown bound to serum proteins. This study, however, showed low urinary excretion of the activity.[63] In addition, the physical size of the Zr complex — especially colloidal or polymeric species — will affect the clearance mechanism, particularly whether or not renal clearance is possible.

When a complex is poorly understood, as in the case of Zr-chloride, the biodistribution behavior can be less definitive as well. For example, one study found that Zr-chloride accumulates in the liver, which suggests it is in a colloidal form[26], while another study using a different preparation method of Zr-chloride showed no accumulation in soft tissue.[62] More stable complexes lead to more straightforward biodistribution data. Zr-phosphate does not demonstrate significant clearance from the body, but instead collects in the liver and spleen, most likely due to precipitation.[62] Zr-DFO is cleared extremely quickly through the kidneys and can be excreted through the urine in a matter of minutes.[26, 54]

Overall, the key to consistent biodistribution and fast, dependable clearance largely rests on the stability and control of the complexation. The stable, organized chelation of Zr-DFO exhibits clear, predictable biological behavior, while the complicated and uncertain speciation of lower denticity complexes leads to problematic or complex biological behavior.

Bone uptake

Zirconium is a bone seeker and so, when not tightly bound to a chelate, accumulates preferentially in bone in both rats[64, 65] and mice[62, 66]. This is a particularly important consideration in the nuclear medicine community, as the accumulation of high levels of ^{89}Zr in bone during clinical scans may act as a dose-limiting characteristic of ^{89}Zr PET agents. A comparison of bone uptake arising from different zirconium species demonstrates that as the denticity and stability of the complexes increases, the bone uptake decreases since the osteophilic Zr^{4+} cation is not released. In practice, this trend translates to the highest bone uptake observed upon the injection of Zr-chloride, followed by Zr-oxalate, then Zr-citrate, and lastly Zr-DFO with significantly less bone uptake (Figure 4). Notably, Zr-phosphate does not show considerable bone uptake comparatively. Additionally, the bone marrow is responsible for much less than one percent (0.1%) of the activity of the bone, while the calcified tissue comprises the bulk of the zirconium uptake with 33% concentrated in the epiphyses.[62] Since free Zr^{4+} is responsible for the observed bone uptake, a more stable chelate for zirconium should further limit the observed bone activity. It is worth noting that early clinical trials with ^{89}Zr do not demonstrate the extent of bone uptake exhibited in preclinical images.

Preclinical Applications

In the past decade, the use of ^{89}Zr for small animal PET imaging has become increasingly widespread and a considerable amount of work has been undertaken at a variety of different institutions (Table 1). By far the most prevalent use of ^{89}Zr lies in the radiolabeling of antibodies due to the favorable match up of the half-life of ^{89}Zr and the circulation time of IgG antibodies.

ImmunoPET

The ability to image a radiolabeled antibody several days after its injection allows for vastly improved image contrast due to decreased background signal. As a residualizing

isotope, ^{89}Zr remains inside cells once the antibody-antigen complex is internalized, allowing activity to accumulate and concentrate in tumors while non-localized activity clears from the body, ultimately resulting in high contrast images. An analysis of each of the individual preclinical studies would, of course, be outside of the scope of this paper; instead, we will provide a few interesting examples to demonstrate the utility of ^{89}Zr in different areas of the preclinical arena.

The potential use of ^{89}Zr immunoPET to monitor and predict the effectiveness of therapy has been demonstrated by Nagengast and co-workers in ovarian cancer using ^{89}Zr-bevacizumab and the HSP90 inhibitor NVP-AUY922.[67] HSP90 inhibition has an antiangiogenic effect and leads to a downstream reduction in the secretion of VEGF which, as this work shows, can be effectively imaged with ^{89}Zr-bevacizumab. The decrease in ^{89}Zr-bevacizumab uptake in A2780 xenografts after treatment with NVP-AUY922 corresponds to the decrease in VEGF levels due to HSP90 inhibition, as confirmed by *in vitro* experiments (Figure 5). Additionally, no such change in uptake was found with CP70 tumors which are known to not respond to AUY922 therapy. Hence, ^{89}Zr-bevacizumab acts as an early biomarker for the effectiveness of HSP90 inhibition and allows for *in vivo* visualization and quantification of early antiangiogenic tumor response.[68]

One recent study demonstrating immediate clinical relevance for castration-resistant prostate cancer was conducted by Ulmert, Evans, and colleagues, who developed a ^{89}Zr-labeled 5A10 antibody targeting free prostate specific antigen (fPSA) that was shown to be able to track intratumoral androgen receptor (AR) signaling due to testosterone levels or pharmacological triggers such as antiandrogen MDV3100 (Figure 6). The clinical importance of PSA levels and the changes thereof has been thoroughly investigated and the ability to non-invasively monitor these changes in the tumor environment could prove greatly beneficial. ^{89}Zr-5A10 is not only able to provide diagnostic imaging of a tumor, but can be used to trace disease progression and evaluate treatment response. Additionally, in contrast to clinically used radiotracers such as ^{99m}Tc-MDP or ^{18}F-NaF, ^{89}Zr-5A10 was able to differentiate cancerous bone metastases from normal bone repair. The ability of this radiotracer to evaluate therapeutic effects and AR-driven tumor activity on the level of individual lesions could be of great value clinically.[65]

Non-Antibody Applications

While immunoPET applications make up the majority of the literature regarding ^{89}Zr-based PET imaging, there is also a growing amount of research into the development of ^{89}Zr-labeled nanomaterials. One such study consists of nanoparticles made up of cross-linked, short chain dextran that were conjugated to p-isothiocyanate DFO for radiolabeling with ^{89}Zr. These dextran nanoparticles (DNPs) are used as imaging probes for macrophages as they are engulfed by mononuclear phagocytic cells. The optimal DNPs tested had an average diameter of 13 nm and were surface modified through succinylation to achieve a blood half-life of 3.9 h. The ^{89}Zr-labeled DNPs were used to image and quantitate tumor-associated macrophages (TAMs) in mice with colon carcinoma xenografts. The resulting PET images showed significant tumor uptake and histology confirmed the co-localization of TAMs and the ^{89}Zr-labeled DNPs at the microscopic level. This methodology represents a step forward in the imaging and understanding of macrophage and inflammation levels associated with cancer and is expected to be helpful in several applications including the evaluation of cancer therapies using antimacrophage strategies. [69]

Challenges

As a longer-lived medical radionuclide, one of the principal concerns regarding the use of ^{89}Zr in the clinic is the substantial radiation dose received by patients compared to

shorter-lived nuclides. However, as long as the radiotracer clears the healthy tissue as expected, the prevailing viewpoint is that the increased diagnostic value is worth the additional dose. Along these lines, a notable issue with ^{89}Zr PET imaging preclinical mouse models is the uptake in bones. The release of osteophilic Zr^{4+} *in vivo* leads to accumulation of the cation in the bone, which can often be seen in the resulting images. Biodistribution results commonly show up to 10% injected dose per gram activity in the bone. Localization of radioactivity in the bone is disadvantageous due to the resulting increased dose to the bone marrow. As discussed earlier, the development of a more favorable zirconium chelate may be the key to reducing this issue.

^{89}Zr-Based Imaging in the Clinic

Despite the youth of the field, the tremendous success of ^{89}Zr-based radiopharmaceuticals in pre-clinical imaging studies with rodent models has led to the rapid clinical translation of a number of ^{89}Zr-labeled antibodies. To date, five reports of clinical investigations using three different ^{89}Zr-labeled antibody conjugates — ^{89}Zr-cmAb-U36, ^{89}Zr-trastuzumab, and ^{89}Zr-ibritumomab tiuxetan — have been presented in the literature.[49, 97-100] Importantly, all of the studies have employed the TFP-*N*-suc-Fe(DFO) conjugation methodology.

The first report of a clinical study employing a ^{89}Zr-labeled antibody was published in 2006 by Börjesson, *et al.*, investigating the safety and diagnostic value of ^{89}Zr-cmAb U36 for the imaging of CD44v6-positive head and neck tumors.[98] In the study, twenty patients with head and neck squamous cell carcinoma (HNSCC) underwent ^{89}Zr-cmAb U36 immunoPET along with CT and/or MRI. The patients received 75 MBq of the ^{89}Zr-labeled conjugate, corresponding to 10 mg of the antibody, and were imaged up to 144 h after injection of the radiopharmaceutical. The authors report that the conjugate was safe (only two of twenty patients developed an antichimeric antibody response), and all primary tumors were detected as well as lymph node metastases in 18 of 25 positive levels (Figure 7). Significantly, the lymph nodes that were missed were determined to be small, contain relatively little tumor tissue, and were often also missed by CT or MRI, resulting in the sensitivity of the immunoPET for lymph node metastases (72%) being comparable if not better to that of CT/MRI (60%). Further, the authors found that in a subset of the patients (n = 6), imaging with ^{89}Zr-cmAb U36 gave comparable results to imaging with ^{18}F-FDG.

In a later report from the same group, both the radiation dosimetry and potential for ^{89}Zr-cmAb-U36 quantification were studied.[97] Here, the authors report that the PET-based quantification of activity in the left ventricle of the heart agreed quite well with values obtained from blood samples; likewise, good correlation between PET- and biopsy-derived values was also observed for tumor uptake. Taken together, these data suggest that ^{89}Zr-cmAb-U36 may be used to quantitatively assess antibody biodistribution, thereby helping to differentiate patients with high and low tumor uptake and in turn aiding in treatment planning. In the same study, the authors determined that the mean effective dose of the immunoPET was 0.53 ± 0.03 mSv/MBq in men and 0.66 ± 0.03 mSv/MBq in women, resulting in an average dose of approximately 40 mSv for the patients in the study receiving 74 mBq. This, of course, is high and could certainly limit the repeated application of ^{89}Zr-immunoPET, though the authors reasonably argue that subsequent studies employing different doses and more modern PET scanners can reduce the dose.

Soon after the first-in-man reports of ^{89}Zr-cmAb-U36, an overlapping group of researchers from the VU Medical Center published a pilot study investigating the use ^{89}Zr-labeled, DFO-modified ibritumomab tiuxetan for monitoring and predicting the biodistribution of ^{90}Y-ibritumomab tiuxetan (Zevalin®) in patients with relapsed or refractory low-grade B-cell non-Hodgkin's lymphoma.[49] The authors report that co-injected ^{89}Zr- and ^{88}Y-

ibritumomab tiuxetan have very comparable biodistributions, despite a few small differences, particularly slightly elevated liver and bone uptake levels for the ^{89}Zr-labeled construct. As a result, they conclude that ^{89}Zr-ibritumomab tiuxetan is well-suited to predict ^{90}Y- ibritumomab tiuxetan dosimetry. More recently, a complementary study has been published illustrating that immunoPET scout scans with ^{89}Zr-ibritumomab tiuxetan prior to radioimmunotherapy with ^{90}Y-ibritumomab tiuxetan can be used to effectively and accurately predict the biodistribution of the ^{90}Y-labeled antibody and the dose-limiting organ during therapy, a development which could aid significantly in patient selection and dose optimization.[99]

In 2010, researchers at the University of Groningen published an investigation into the use of ^{89}Zr-trastuzumab for imaging Her2-positive lesions in patients with metastatic breast cancer.[100, 101] In the study, the patients (n = 14 total) were divided into three groups that received 10 or 50 mg of trastuzumab for antibody-naïve patients or 10 mg for patients on trastuzumab treatment. It was found that for the trastuzumab-naïve patients, a 50 mg dose of ^{89}Zr-trastuzumab was required for effective imaging, while a 10 mg dose was sufficient for patients on trastuzumab treatment. The ^{89}Zr-trastuzumab produced excellent images, with high spatial resolution and good signal-to-noise ratio as well as high tumor uptake. It also allowed for the observation of metastatic lesions in the liver, lung, bone, and brain (Figure 8). The uptake in brain lesions was particularly interesting, a result that is both suggestive of the breakdown of the blood brain barrier in the patients studied and indicative of the utility of ^{89}Zr-trastuzumab and other ^{89}Zr-labeled antibodies for the imaging of brain tumors. The authors report that the most favorable imaging times were 4-5 d after injection of the radiopharmaceutical, and while a full study between imaging modalities was not conducted, the immunoPET results generally correlated well with complementary imaging with CT, MRI, and bone scans. Finally, and importantly, the radiation dose to patients was significantly attenuated in this study compare to the ^{89}Zr-cmAb-U36 investigations: patients received 37 MBq ^{89}Zr-trastuzumab for an average dose of 20 mSv.

As of this writing, all of the published clinical investigations with ^{89}Zr-labeled antibodies have been performed in the Netherlands; however, the rapid advent of ^{89}Zr-based immunoPET means this will certainly cease to be the case. At Memorial Sloan-Kettering Cancer Center, for example, a pilot study focuses on the use of ^{89}Zr-J591 for the detection of prostate-specific membrane antigen-positive lesions in castrate-resistant prostate cancer patients. Data collection is still underway, though results from the first few patients are very promising: the ^{89}Zr-J591 displays high spatial resolution in addition to uptake both in primary tumors and distant metastases (Figure 9).

Conclusions

In the preceding pages, we have hoped to illustrate to the reader both the depth and breadth of the research in the rapidly expanding field of ^{89}Zr-based PET imaging, with investigations ranging from basic metal coordination chemistry to on-going clinical trials. Indeed, the field is proceeding at such an exciting pace that important contributions to our knowledge of ^{89}Zr-PET will no doubt be made between the writing of this manuscript and its ultimate publication. Yet despite the manifold successes, much work is to be done as this field grows and matures. In particular, we believe that emphasis should be placed on five areas: (A) the synthesis and evaluation of novel chelators that strike a balance between rapid coordination kinetics and high thermodynamic stability in order to address the observed *in vivo* release of ^{89}Zr^{4+} and its subsequent mineralization in the bone; (B) the development of mild, modular, and site-specific bioconjugation strategies with which to attach DFO to antibodies; (C) the expansion of ^{89}Zr-based PET imaging from antibodies to other targeting vectors with suitable pharmacokinetics; (D) the advancement of our understanding of the *in*

vivo metabolism of $^{89}Zr^{4+}$-labeled bioconjugates; and finally, but perhaps most important, (E) the performance of direct comparison studies between ^{89}Zr-labeled antibodies and antibodies labeled with other relevant isotopes in both pre-clinical models and a clinical environment to allow for the quantitative and comprehensive comparison between ^{89}Zr-immunoPET and its competitor modalities.

As these issues are addressed, new ^{89}Zr-labeled radiopharmaceuticals are developed, and new pre-clinical and clinical studies are performed, we believe that ^{89}Zr-based PET imaging will continue to progress, expand to involve new disciplines and address different pathologies, and ultimately take an extremely important place at the forefront of medical imaging.

Acknowledgments

First and foremost, the authors would like to thank all of those researchers whose work has contributed to the science discussed in these pages. The authors also thank Dr. Pat Zanzonico, Lawanya Singh, and Lauren Hannah for helpful discussions. Finally, the authors thank the NIH (BMZ, Award 1F32CA1440138-01), NSF (MAD, IGERT 0965983), and Geoffrey Beene Cancer Research Center of Memorial Sloan- Kettering Cancer Center for their generous funding support.

References

1. Wu AM, Senter PD. Arming antibodies: prospects and challenges for immunoconjugates. Nat Biotech. 2005; 23:1137–46.
2. Wu AM, Olafsen T. Antibodies for molecular imaging of cancer. Cancer J. 2008; 14:191–7. [PubMed: 18536559]
3. Zeglis BM, Lewis JS. A practical guide to the construction of radiometallated bioconjugates for positron emission tomography. Dalton T. 2011; 40:6168–95.
4. Wadas TJ, Wong EH, Weisman GR, Anderson CJ. Coordinating radiometals of copper, gallium, indium, yttrium, and zirconium for PET and SPECT imaging of disease. Chem Rev. 2010; 110:2858–902. [PubMed: 20415480]
5. Anderson CJ, Connett JM, Schwarz SW, Rocque PA, Guo LW, Philpott GW, et al. Copper-64-labeled antibodies for PET imaging. J Nucl Med. 1992; 33:1685–90. [PubMed: 1517844]
6. Cai WB, Chen K, He LN, Cao QH, Koong A, Chen XY. Quantitative PET of EGFR expression in xenograft-bearing mice using Cu-64-labeled cetuximab, a chimeric anti-EGFR monoclonal antibody. Eur J Nucl Med Mol I. 2007; 34:850–8.
7. Niu G, Li Z, Cao Q, Chen X. Monitoring therapeutic response of human ovarian cancer with 17-DMAG by noninvasive PET imaging with ^{64}Cu-DOTA-trastuzumab. Eur J Nucl Med Mol I. 2009; 36:1510–9.
8. Paudyal P, Paudyal B, Hanaoka H, Oriuchi N, Iida Y, Yoshioka H, et al. Imaging and biodistribution of Her2/neu expression in non-small cell lung cancer xenografts with 64Cu-labeled trastuzumab PET. Cancer Sci. 2010; 101:1045–50. [PubMed: 20219072]
9. Carrasquillo JA, Pandi-Taskar N, O'Donoghue JA, Humm JL, Zanzonico P, Smith-Jones PM, et al. 124I-huA33 antibody PET of colorectal cancer. J Nucl Med. 2011; 52:1173–80. [PubMed: 21764796]
10. Verel I, Visser GWM, Vosjan MJWD, Finn R, Boellaard R, Van Dongen GAMS. High-quality 124I-labelled monoclonal antibodies for use as PET scouting agents prior to 131I-radioimmunotherapy. Eur J Nucl Med Mol I. 2004; 31:1645–52.
11. Dijkers ECF, Kosterink JGW, Rademaker AP, Perk LR, van Dongen GAMS, Bart J, et al. Development and characterization of clinical-grade 89Zr-trastuzumab for HER2/neu immunolPET imaging. J Nucl Med. 2009; 50:974–81. [PubMed: 19443585]
12. Munnink THO, de Korte MA, Nagengast WB, Timmer-Bosscha H, Schroder CP, de Jong JR, et al. Zr-89-trastuzumab PET visualises HER2 downregulation by the HSP90 inhibitor NVP-AUY922 in a human tumour xenograft. Eur J Cancer. 2010; 46:678–84. [PubMed: 20036116]

13. Perk LR, Visser GWM, Vosjan M, Stigter-van Walsum M, Tijink BM, Leemans CR, et al. Zr-89 as a PET surrogate radioisotope for scouting biodistribution of the therapeutic radiometals Y-90 and Lu-117 in tumor-bearing nude mice after coupling to the internalizing antibody cetuximab. J Nucl Med. 2005; 46:1898–906. [PubMed: 16269605]
14. Perk LR, Visser OJ, Walsum MSV, Vosjan M, Visser GWM, Zijlstra JM, et al. Preparation and evaluation of Zr-89-Zevalin for monitoring of Y-90-Zevalin biodistribution with positron emission tomography. Eur J Nucl Med Mol I. 2006; 33:1337–45.
15. Holland JP, Sheh YC, Lewis JS. Standardized methods for the production of high specific-activity zirconium-89. Nucl Med Bio. 2009; 36:729–39. [PubMed: 19720285]
16. Holland JP, Williamson MJ, Lewis JS. Unconventional Nuclides for Radiopharmaceuticals. Mol Imaging. 2010; 9:1–20. [PubMed: 20128994]
17. Vugts DJ, Van Dongen G. 89Zr-labeled compounds for PET imaging guided personalized therapy. Drug Discov Today. 2011; 8:e53–e61.
18. Severin GW, Engle JW, Barnhart TE, Nickles RJ. Zr-89 radiochemistry for positron emission tomography. Med Chem. 2012; 7:389–94. [PubMed: 21711221]
19. Hohn A, Zimmermann K, Schaub E, Hirzel W, Schubiger PA, Schibli R. Production and separation of “non-standard” PET nuclides at a large cyclotron facility: the experiences at the Paul Scherrer Institute in Switzerland. Q J Nucl Med Mol Im. 2008; 52:145–50.
20. Zhang Y, Hong H, Cai W. PET tracers based on zirconium-89. Current Radiopharm. 2011; 4:131–9.
21. Rice SL, Roney CA, Daumar P, Lewis JS. The next generation of positron emission tomography radiopharmaceuticals in oncology. Semin Nucl Med. 2011; 41:265–82. [PubMed: 21624561]
22. Ikotun OF, Lapi SE. The rise of metal radionuclides in medical imaging: copper-64, zirconium-89 and yttrium-86. Future Med Chem. 2011; 3:599–621. [PubMed: 21526898]
23. Zeglis B, Lewis JS. A practical guide to the construction of radiometallation bioconjugates for positron emission tomography. Dalton T. 2011; 40:6168–95.
24. Shore FJ, Bendel WL, Brown HN, Becker RA. Radiations from Zr-89. Phys Rev. 1953; 91:1203–11.
25. Dejesus OT, Nickles RJ. Production and purification of Zr-89, a potential PET antibody label. Appl Radiat Isotopes. 1990; 41:789–90.
26. Holland JP, Sheh Y, Lewis JS. Standardized methods for the production of high specific-activity zirconium-89. Nucl Med Bio. 2009; 36:729–39. [PubMed: 19720285]
27. Ruggiero A, Holland JP, Lewis JS, Grimm J. Cerenkov luminescence imaging of medical isotopes. J Nucl Med. 2010; 51:1123–30. [PubMed: 20554722]
28. Hinrichsen PF. Decay of 78.4 h 89Zr. Nucl Phys. 1968; A118:538–44.
29. Meijs WE, Herscheid JDM, Haisma HJ, Wijbrandts R, Vanlangevelde F, Vanleuffen PJ, et al. Production of highly pure no-carrier added Zr-89 for the labeling of antibodies with a positron emitter. Appl Radiat Isotopes. 1994; 45:1143–7.
30. Omara HM, Hassan KF, Kandil SA, Hegazy FE, Saleh ZA. Proton induced reactions on Y-89 with particular reference to the production of the medically interesting radionuclide Zr-89. Radiochim Acta. 2009; 97:467–71.
31. Zweit J, Downey S, Sharma HL. Production of no-carrier-added zirconium-89 for positron emission tomography. Appl Radiat Isotopes. 1991; 42:199–201.
32. Dutta B, Maiti M, Lahiri S. Production of Zr-88,Zr-89 by proton induced activation of Y-nat and separation by SLX and LLX. J Radioanal Nucl Chem. 2009; 281:663–7.
33. Verel I, Visser GWM, Boellaard R, Stigter-van Walsum M, Snow GB, van Dongen G. Zr-89 immuno-PET: Comprehensive procedures for the production of Zr-89-labeled monoclonal antibodies. J Nucl Med. 2003; 44:1271–81. [PubMed: 12902418]
34. Multi-Agency Radiological Laboratory Analytical Protocols Manual (NUREG-1576, Initial Report). 2004. p. 14-191.
35. Shannon RD. Revised effective ionic radii and systematic studies of interatomic distances in halides and chalcogenides. Acta Crystallogr A. 1976; 32:751–67.

36. Ekberg C, Källvenius G, Albinsson Y, Brown PL. Studies on the hydrolytic behavior of zirconium(IV). J Solution Chem. 2004; 33:47–79.
37. Singhal A, Toth LM, Lin JS, Affholter K. Zirconium(IV) tetramer/octamer hydrolysis equilibrium in aqueous hydrochloric acid solution. J Am Chem Soc. 1996; 118:11529–34.
38. Lee DB, Roberts M, Bluchel CG, Odell RA. Zirconium: biomedical and nephrological applications. ASAIO J. 2010; 56:550–6. [PubMed: 21245802]
39. Matsui S, Mitani M, Saito J, Tohi Y, Makio H, Matsukawa N, et al. A family of zirconium complexes having two phenoxy–imine chelate ligands for olefin polymerization. J Am Chem Soc. 2001; 123:6847–56.
40. Ning Y, Zhang Y, Rodriguez-Delgado A, Chen EYX. Neutral metallocene ester enolate and non-metallocene alkoxy complexes of zirconium for catalytic ring-opening polymerization of cyclic esters. Organometallics. 2008; 27:5632–40.
41. Reznichenko AL, Hultzsch KC. C-2-Symmetric zirconium bis(amidate) complexes with enhanced reactivity in aminoalkene hydroamination. Organometallics. 2010; 29:24–7.
42. Zhang Z-H, Li T-S. Applications of zirconium (IV) compounds in organic synthesis. Curr Org Chem. 2009; 13:1–30.
43. Gornshtein F, Kapon M, Botoshansky M, Eisen MS. Titanium and zirconium complexes for polymerization of propylene and cyclic esters. Organometallics. 2007; 26:497–507.
44. Stephan DW. Zirconium-phosphorus chemistry: Strategies in syntheses, reactivity, catalysis, and utility. Angew Chem Int Edit. 2000; 39:314–29.
45. Pozhidaev AI, Porai-Koshits MA, Polynova TN. Crystal structure of zirconium ethylenediaminetetraacetate tetrahydrate. J Struct Chem. 1974; 15:548–53.
46. Ilyukhin AB, Davidovich RL, Samsonova IN, Teplukhina LV. Eightfold-coordinated diethylenetriaminepentaacetates: Crystal structures of K[M(Dtpa)]center dot 3H(2)O (M = Zr or Hf) and NH4[Sn(Dtpa)]center dot H2O. Crystallogr. Rep. 2000; 45:39–43.
47. Parker D, Pulukkody K, Smith FC, Batsanov A, Howard JAK. Structures of the yttrium complexes of 1,4,7,10-tetraazacyclododecane-N,N[prime or minute],N[double prime],N[triple prime]-tetraacetic acid (H4dota) and N,N[double prime]-bis(benzylcarbamoylmethyl)diethylenetriamine-N,N[prime or minute],N[double prime]-triacetic acid and the solution structure of a zirconium complex of H4dota. J Chem Soc Dalton. 1994:689–93.
48. Martell, AE.; Smith, RM. Critical Stability Constants. Plenum Press; New York: 1974.
49. Perk LR, Visser OJ, Walsum MS-v, Vosjan MJWD, Visser GWM, Zijlstra JM, et al. Preparation and evaluation of Zr-89-Zevalin for monitoring of Y-90-Zevalin biodistribution with positron emission tomography. Eur J Nucl Med Mol I. 2006; 33:1337–45.
50. Baroncelli F, Grossi G. The complexing power of hydroxamic acids and its effect on the behaviour of organic extractants in the reprocessing of irradiated fuels—I the complexes between benzohydroxamic acid and zirconium, iron (III) and uranium (VI). J Inorg Nucl Chem. 1965; 27:1085–92.
51. Meijs WE, Herscheid JDM, Haisma HJ, Pinedo HM. Evaluation of desferal as a bifunctional chelating agent for labeling antibodies with Zr-89. Appl Radiat Isotopes. 1992; 43:1443–7.
52. Holland JP, Divilov V, Bander NH, Smith-Jones PM, Larson SM, Lewis JS. Zr-89-DFO-J591 for immunoPET of prostate-specific membrane antigen expression in vivo. J Nucl Med. 2010; 51:1293–300. [PubMed: 20660376]
53. Koizumi M, Endo K, Kunimatsu M, Sakahara H, Nakashima T, Kawamura Y, et al. Preparation of 67Ga-labeled antibodies using deferoxamine as a bifunctional chelate an improved method. J Immunol Methods. 1987; 104:93–102. [PubMed: 3316401]
54. Meijs WE, Haisma HJ, VanderSchors R, Wijbrandts R, VandenOever K, Klok RP, et al. A facile method for the labeling of proteins with zirconium isotopes. Nucl Med Bio. 1996; 23:439–48. [PubMed: 8832698]
55. Lewis MR, Shively JE. Maleimidocysteineamido-DOTA Derivatives: New reagents for radiometal chelate conjugation to antibody sulfhydryl groups undergo pH-dependent cleavage reactions. Bioconjugate Chem. 1998; 9:72–86.
56. Perk LR, Vosjan MJWD, Visser GWM, Budde M, Jurek P, Kiefer GE, et al. p-Isothiocyanatobenzyl-desferrioxamine: a new bifunctional chelate for facile radiolabeling of

monoclonal antibodies with zirconium-89 for immuno-PET imaging. Eur J Nucl Med Mol I. 2010; 37:250–9.

57. Vosjan MJWD, Perk LR, Visser GWM, Budde M, Jurek P, Kiefer GE, et al. Conjugation and radiolabeling of monoclonal antibodies with zirconium-89 for PET imaging using the bifunctional chelate p-isothiocyanatobenzyl-desferrioxamine. Nat Protoc. 2010; 5:739–43. [PubMed: 20360768]
58. Tinianow JN, Gill HS, Ogasawara A, Flores JE, Vanderbilt AN, Luis E, et al. Site-specifically Zr-89-labeled monoclonal antibodies for ImmunoPET. Nucl Med Bio. 2010; 37:289–97. [PubMed: 20346868]
59. Zeglis BM, Mohindra P, Weissmann GI, Divilov V, Hilderbrand SA, Weissleder R, et al. Modular strategy for the construction of radiometalated antibodies for positron emission tomography based on inverse electron demand diels–alder click chemistry. Bioconjugate Chem. 2011; 22:2048–59.
60. Vugts DJ, Vervoort A, Stigter-van Walsum M, Visser GWM, Robillard MS, Versteegen RM, et al. Synthesis of phosphine and antibody-azide probes for in vivo staudinger ligation in a pretargeted imaging and therapy approach. Bioconjugate Chem. 2011; 22:2072–81.
61. McClinton LT, Schubert J. The toxicity of some zirconium and thorium salts in rats. J Pharmacol Exp Ther. 1948; 94:1–6. [PubMed: 18885606]
62. Abou DS, Ku T, Smith-Jones PM. In vivo biodistribution and accumulation of 89Zr in mice. Nucl Med Bio. 2011; 38:675–81. [PubMed: 21718943]
63. Mealey J. Turn-over of carrier-free zirconium-89 in Man. Nature. 1957; 179:673–4. [PubMed: 13418761]
64. Rama Sastry BV, Owens LK, Ball COT. Differences in the distribution of zirconium-95 and niobium-95 in the rat. Nature. 1964; 201:410–1. [PubMed: 14110018]
65. CR F. The radiological hazards of zirconium-95 and niobium-95. Health Phys. 1969; 16:209–20. [PubMed: 5772185]
66. Meijs WE, Haisma HJ, Klok RP, vanGog FB, Kievit E, Pinedo HM, et al. Zirconium-labeled monoclonal antibodies and their distribution in tumor-bearing nude mice. J Nucl Med. 1997; 38:112–8. [PubMed: 8998164]
67. Munnink THO, de Korte MA, Nagengast WB, Timmer-Bosscha H, Schroder CP, de Jong JR, et al. Zr-89-trastuzumab PET visualises HER2 downregulation by the HSP90 inhibitor NVP-AUY922 in a human tumour xenograft. Eur J Cancer. 2010; 46:678–84. [PubMed: 20036116]
68. Nagengast WB, de Korte MA, Munnink THO, Timmer-Bosscha H, den Dunnen WF, Hollema H, et al. (89)Zr-bevacizumab PET of early antiangiogenic tumor response to treatment with HSP90 inhibitor NVP-AUY922. J Nucl Med. 2010; 51:761–7. [PubMed: 20395337]
69. Keliher EJ, Yoo J, Nahrendorf M, Lewis JS, Marinelli B, Newton A, et al. 89Zr-Labeled dextran nanoparticles allow in vivo macrophage imaging. Bioconjugate Chem. 2011; 22:2383–9.
70. Aerts HJWL, Dubois L, Perk L, Vermaelen P, van Dongen GAMS, Wouters BG, et al. Disparity between in vivo EGFR expression and (89)Zr-labeled cetuximab uptake Assessed with PET. J Nucl Med. 2009; 50:123–31. [PubMed: 19091906]
71. Cohen R, Stammes MA, de Roos IH, Stigter-van Walsum M, Visser GW, van Dongen GA. Inert coupling of IRDye800CW to monoclonal antibodies for clinical optical imaging of tumor targets. Eur J Nucl Med Mol I. 2011; 1:31.
72. Perk LR, Visser GW, Vosjan MJ, Stigter-van Walsum M, Tijink BM, Leemans CR, et al. (89)Zr as a PET surrogate radioisotope for scouting biodistribution of the therapeutic radiometals (90)Y and (177)Lu in tumor-bearing nude mice after coupling to the internalizing antibody cetuximab. J Nucl Med. 2005; 46:1898–906. [PubMed: 16269605]
73. Hong H, Severin GW, Yang Y, Engle JW, Zhang Y, Barnhart TE, et al. Positron emission tomography imaging of CD105 expression with 89Zr-Df-TRC105. Eur J Nucl Med Mol I. 2012; 39:138–48.
74. Nagengast WB, de Vries EG, Hospers GA, Mulder NH, de Jong JR, Hollema H, et al. In vivo VEGF imaging with radiolabeled bevacizumab in a human ovarian tumor xenograft. J Nucl Med. 2007; 48:1313–9. [PubMed: 17631557]
75. van Scheltinga AGTT, van Dam GM, Nagengast WB, Ntziachristos V, Hollema H, Herek JL, et al. Intraoperative near-infrared fluorescence tumor imaging with vascular endothelial growth factor

and human epidermal growth factor receptor 2 targeting a ntibodies. J Nucl Med. 2011; 52:1778–85. [PubMed: 21990576]

76. Holland JP, Normand G, Ruggiero A, Lewis JS, Grimm J. Intraoperative imaging of positron emission tomographic radiotracers using cerenkov luminescence emissions. Mol Imaging. 2011; 10:177–185. [PubMed: 21496448]
77. Holland JP, Caldas-Lopes E, Divilov V, Longo VA, Taldone T, Zatorska D, et al. Measuring the pharmacodynamic effects of a novel Hsp90 inhibitor on HER2/neu expression in mice using 89Zr-DFO-trastuzumab. PLoS ONE. 2010; 5:e8859. [PubMed: 20111600]
78. Ruggiero A, Holland JP, Lewis JS, Grimm J. Cerenkov luminescence imaging of medical isotopes. J Nucl Med. 2010; 51:1123–30. [PubMed: 20554722]
79. Verel I, Visser GWM, Boellaard R, Boerman OC, van Eerd J, Snow GB, et al. Quantitative Zr-89 immuno-PET for in vivo scouting of Y-90-labeled monoclonal antibodies in xenograft- bearing nude mice. J Nucl Med. 2003; 44:1663–70. [PubMed: 14530484]
80. Verel I, Visser GWM, Boerman OC, van Eerd JEM, Finn R, Boellaard R, et al. Long-lived positron emitters zirconium-89 and iodine-124 for scouting of therapeutic radioimmunoconjugates with PET. Cancer Biother Radio. 2003; 18:655–61.
81. Brouwers A, Verel I, Van Eerd J, Visser G, Steffens M, Oosterwijk E, et al. PET radioimmunoscintigraphy of renal cell cancer using Zr-89-labeled cG250 monoclonal antibody in nude rats. Cancer Biother Radio. 2004; 19:155–63.
82. Heskamp S, van Laarhoven HWM, Molkenboer-Kuenen JDM, Franssen GM, Versleijen-Jonkers YMH, Oyen WJG, et al. ImmunoSPECT and immunoPET of IGF-1R expression with the radiolabeled antibody R1507 in a triple-negative breast Cancer model. J Nucl Med. 2010; 51:1565–72. [PubMed: 20847162]
83. Munnink THO, Arjaans MEA, Timmer-Bosscha H, Schroder CP, Hesselink JW, Vedelaar SR, et al. PET with the Zr-89-labeled transforming growth factor-beta antibody fresolimumab in tumor models. J Nucl Med. 2011; 52:2001–8. [PubMed: 22072706]
84. Perk LR, Walsum MS-v, Visser GWM, Kloet RW, Vosjan MJWD, Leemans CR, et al. Quantitative PET imaging of Met-expressing human cancer xenografts with Zr-89-labelled monoclonal antibody DN30. Eur J Nucl Med Mol I. 2008; 35:1857–67.
85. Ruggiero A, Holland JP, Hudolin T, Shenker L, Koulova A, Bander NH, et al. Targeting the internal epitope of prostate-specific membrane antigen with Zr-89-7E11 immuno-PET. J Nucl Med. 2011; 52:1608–15. [PubMed: 21908391]
86. van Rij CM, Sharkey RM, Goldenberg DM, Frielink C, Molkenboer JD, Franssen GM, et al. Imaging of prostate cancer with immuno-PET and immuno-SPECT using a radiolabeled anti-EGP-1 monoclonal antibody. J Nucl Med. 2011; 52:1601–7. [PubMed: 21865288]
87. Nayak TK, Garmestani K, Milenic DE, Brechbiel MW. PET and MRI of metastatic peritoneal and pulmonary colorectal cancer in mice with human epidermal growth factor receptor 1-targeted 89Zr-labeled panitumumab. J Nucl Med. 2012; 53:113–20. [PubMed: 22213822]
88. Walther M, Gebhardt P, Grosse-Gehling P, Wuerbach L, Irmler I, Preusche S, et al. Implementation of Zr-89 production and in vivo imaging of B-cells in mice with Zr-89-labeled anti-B-cell antibodies by small animal PET/CT. Appl Radiat Isotopes. 2011; 69:852–7.
89. Vosjan MJWD, Vercammen J, Kolkman JA, Stigter-van Walsum M, Revets H, van Dongen GAMS. Nanobodies targeting the hepatocyte growth factor: potential new drugs for molecular cancer therapy. Mol Cancer Ther. 2012; 11:1017–25. [PubMed: 22319202]
90. Nagengast WB, Lub-de Hooge MN, Oosting SF, den Dunnen WFA, Warnders F-J, Brouwers AH, et al. VEGF-PET imaging is a noninvasive biomarker showing differential changes in the tumor during sunitinib treatment. Cancer Res. 2011; 71:143–53. [PubMed: 21084271]
91. Hoeben BAW, Kaanders JHAM, Franssen GM, Troost EGC, Rijken PFJW, Oosterwijk E, et al. PET of hypoxia with Zr-89-labeled cG250-F(ab ')(2) in head and neck tumors. J Nucl Med. 2010; 51:1076–83. [PubMed: 20554724]
92. Jacobson O, Zhu L, Niu G, Weiss ID, Szajek LP, Ma Y, et al. MicroPET imaging of integrin alpha(v)beta(3) expressing tumors using Zr-89-RGD peptides. Mol Imaging Biol. 2011; 13:1224–33. [PubMed: 21161690]

93. Heneweer C, Holland JP, Divilov V, Carlin S, Lewis JS. Magnitude of enhanced permeability and retention effect in tumors with different phenotypes: Zr-89-albumin as a model system. J Nucl Med. 2011; 52:625–33. [PubMed: 21421727]

94. Avila-Rodriguez MA, Selwyn RG, Hampel JA, Thornadsen BR, DeJesus OT, Converse AK, et al. Positron-emitting resin microspheres as surrogates of Y-90 SIR-Spheres: a radiolabeling and stability study. Nucl Med Bio. 2007; 34:585–90. [PubMed: 17591559]

95. Heuveling DA, Visser GWM, Baclayon M, Roos WH, Wuite GJL, Hoekstra OS, et al. Zr-89-Nanocolloidal albumin-based PET/CT lymphoscintigraphy for sentinel node detection in head and neck cancer: preclinical results. J Nucl Med. 2011; 52:1580–4. [PubMed: 21890880]

96. Ruggiero A, Villa CH, Holland JP, Sprinkle SR, May C, Lewis JS, et al. Imaging and treating tumor vasculature with targeted radiolabeled carbon nanotubes. Int J Nanomed. 2010; 5:783–802.

97. Boerjesson PKE, Jauw YWS, de Bree R, Roos JC, Castelijns JA, Leemans CR, et al. Radiation dosimetry of Zr-89-labeled chimeric monoclonal antibody U36 as used for immuno-PET in head and neck cancer patients. J Nucl Med. 2009; 50:1828–36. [PubMed: 19837762]

98. Borjesson PKE, Jauw YWS, Boellaard R, de Bree R, Comans EFI, Roos JC, et al. Performance of immuno-positron emission tomography with zirconium-89-labeled chimeric monoclonal antibody U36 in the detection of lymph node metastases in head and neck cancer patients. Clin Cancer Rese. 2006; 12:2133–40.

99. Rizvi SNF, Visser OJ, Vosjan MJWD, van Lingen A, Hoekstra OS, Zijlstra JM, et al. Biodistribution, radiation dosimetry and scouting of Y-90-ibritumomab tiuxetan therapy in patients with relapsed B-cell non-Hodgkin's lymphoma using Zr-89-ibritumomab tiuxetan and PET. Eur J Nucl Med Mol I. 2012; 39:512–20.

100. Dijkers EC, Munnink THO, Kosterink JG, Brouwers AH, Jager PL, de Jong JR, et al. Biodistribution of Zr-89-trastuzumab and PET imaging of HER2-positive lesions in patients with metastatic breast cancer. Clin Pharmacol Ther. 2010; 87:586–92. [PubMed: 20357763]

101. Dijkers ECF, Kosterink JGW, Rademaker AP, Perk LR, van Dongen GAMS, Bart J, et al. Development and characterization of clinical-grade Zr-89-trastuzumab for HER2/neu immunoPET imaging. J Nucl Med. 2009; 50:974–81. [PubMed: 19443585]

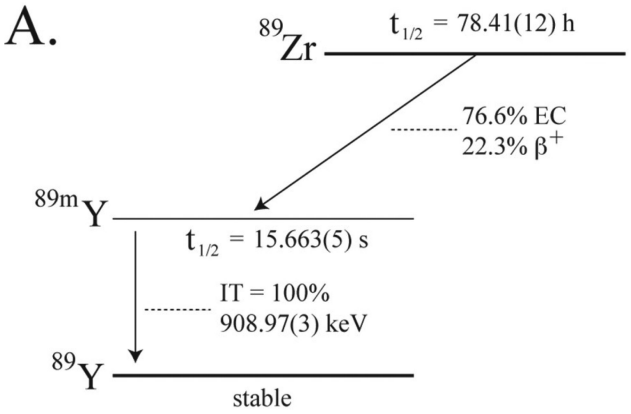

B.

Half-life	87.4(12) h
Decay Mode	ε = 76.6% β^+ = 22.3%
E(β^+)	395.5(11) keV
β^+end-point energy (keV)	902(3) keV
Abundance, I_{β^+}/%	22.74(24)
E_γ/keV (intensity, I_γ/%)	511.0 (45.5%) 909.2 (99.0%)

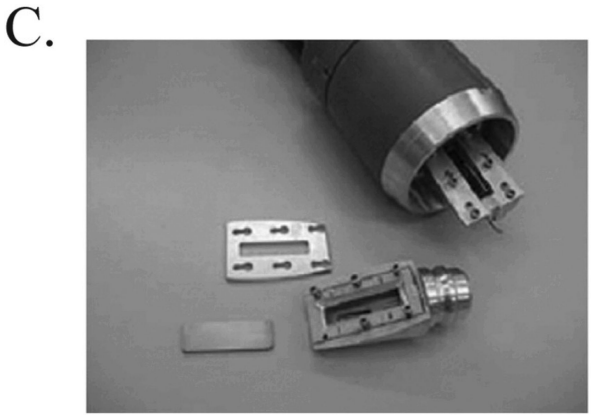

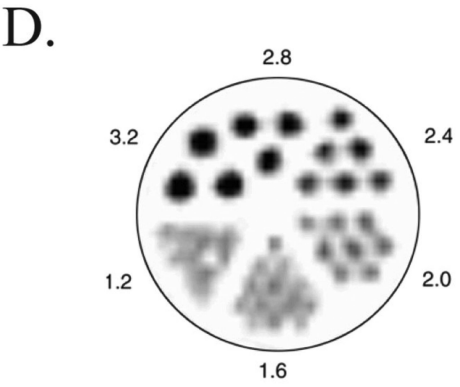

Figure 1.

(A) A simplified decay scheme of ^{89}Zr; (B) Some salient decay characteristics of ^{89}Zr; (C) Photograph of the custom-made water-cooled solid-target assembly for the TR19/9 cyclotron used at Memorial Sloan-Kettering Cancer; (D) A static 10 minute PET image recorded by using a Derenzo phantom, with corresponding hole diameters in mm. (C) and (D) are modified and reprinted from Holland, *et al.* Nucl Med Bio 2009; 36:729-39.

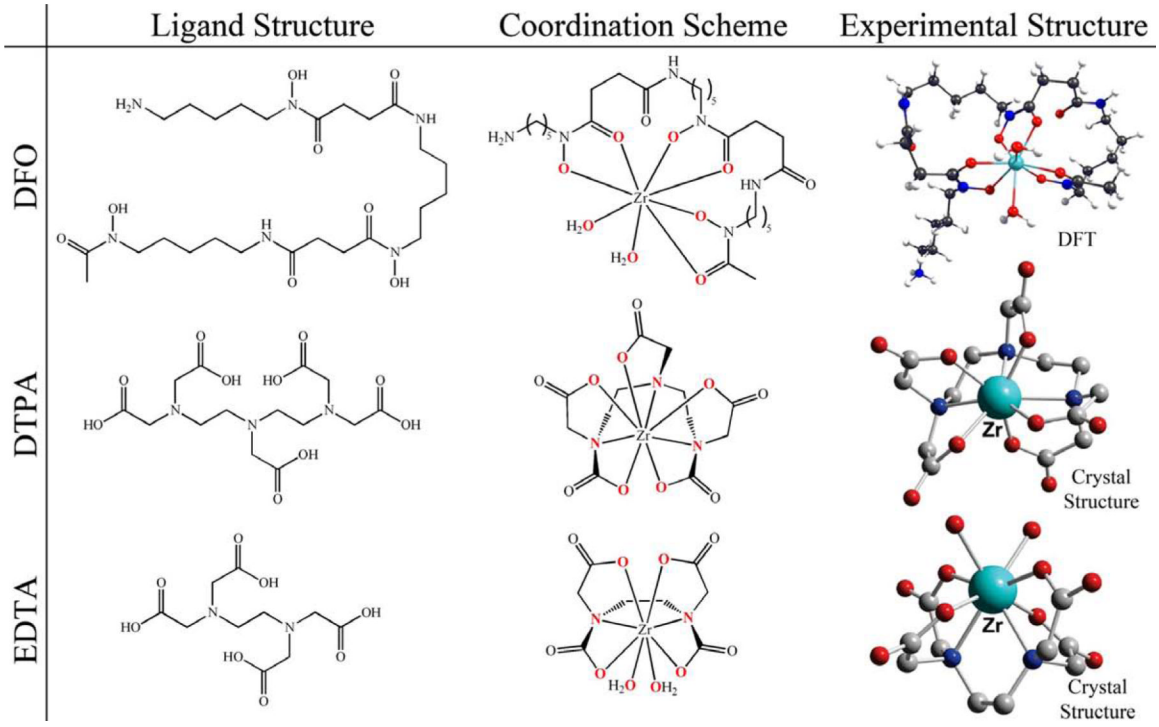

Figure 2.
The ligand structure, coordination scheme, and experimental structure of some commonly-employed chelators for Zr^{4+} and their complexes with the metal.

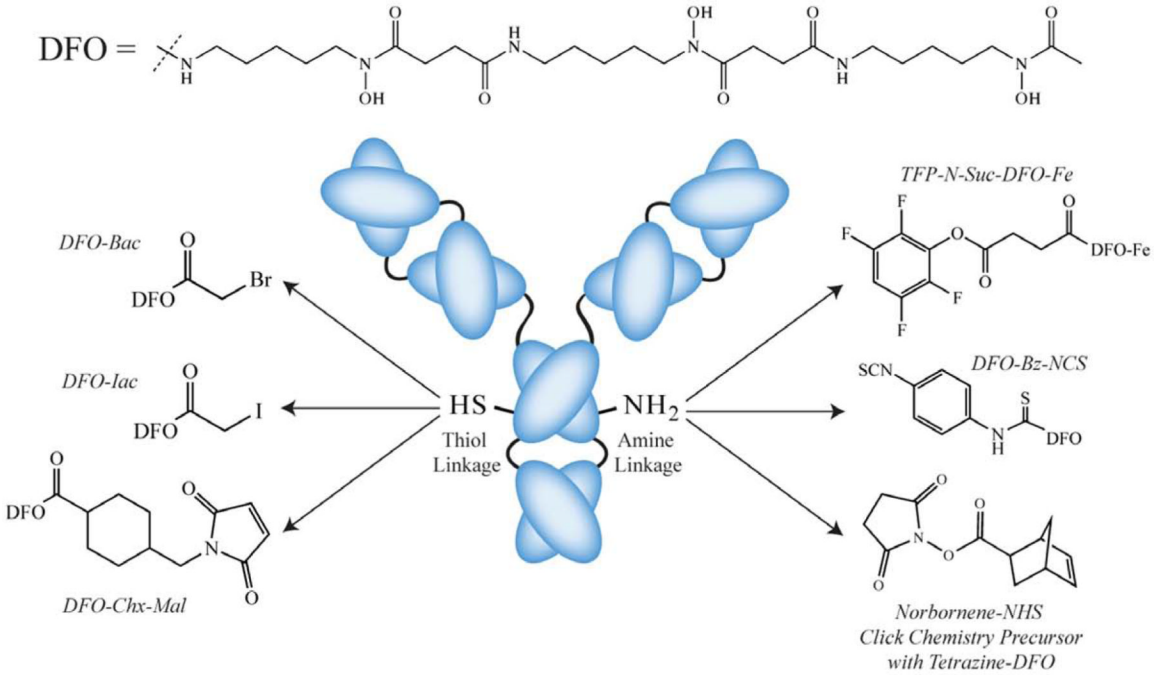

Figure 3.
Schematic of some common DFO conjugation strategies.

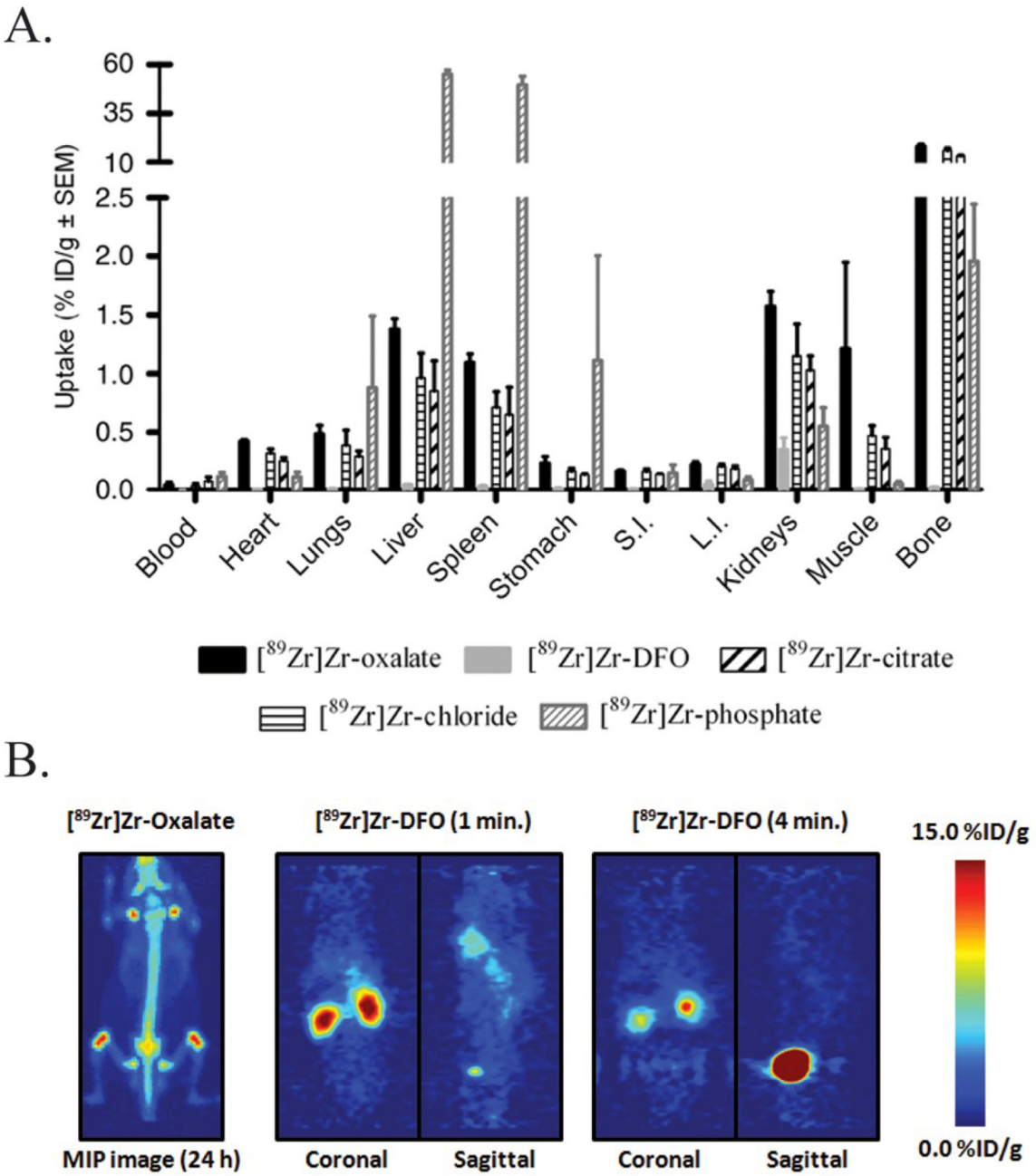

Figure 4.

(A) Biodistribution of radioactivity at 6 days post-injection following i.v. administration of various chemical form of ^{89}Zr in female NIH Swiss mice (n ≥ 3; note the axis break). Reprinted with permission from Abou, *et al.* Nucl Med Bio 2011;38:675-81. (B) PET images showing maximum intensity projection of ^{89}Zr-oxalate at 24 h after intravenous administration and dynamic PET images of ^{89}Zr-DFO at 1 and 4 min after injection. Adapted with permission from Holland, *et al.* J Nucl Med 2010; 51: 1293-300.

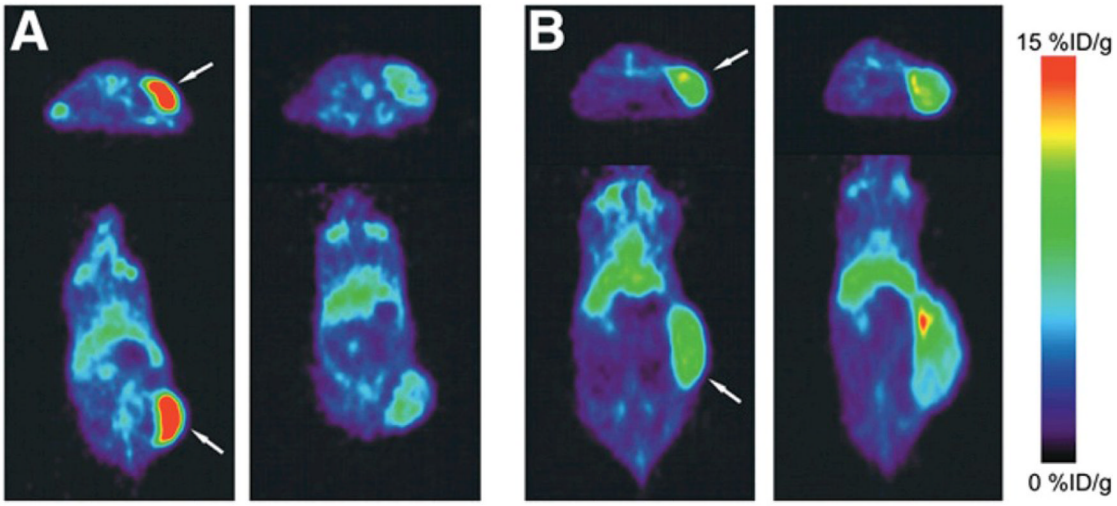

Figure 5.
Representative transversal and coronal small animal PET images of ^{89}Zr-bevacizumab obtained before treatment of A2780 (A) and CP70 (B) xenografts (left) and after NVP-AUY922 treatment (right). Images were obtained at 144 h after injection of 89Zr-bevacizumab. Tumor is indicated by arrow. Reprinted with permission from Nagengast, *et al.* J Nucl Med 2010; 51: 761-767.

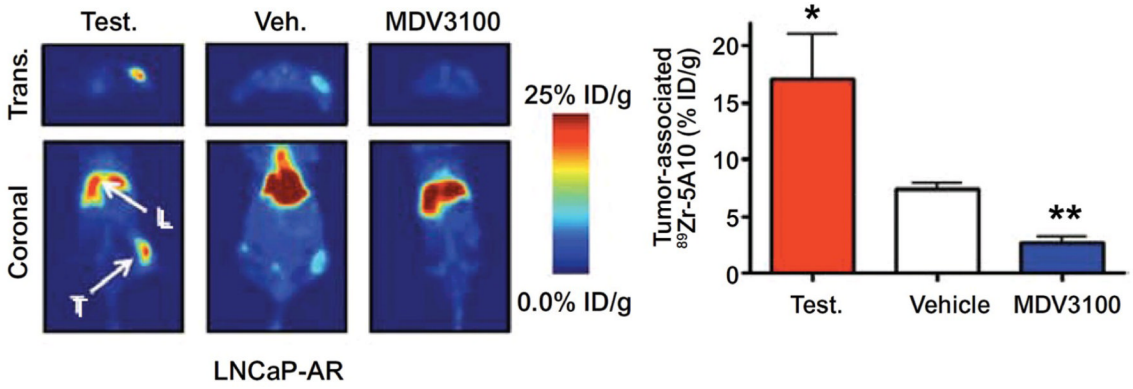

Figure 6.

^{89}Zr-5A10 detects pharmacologic inhibition of AR *in vivo* Left: representative transverse and coronal PET slices of intact male mice bearing LNCaP-AR xenografts on the right flank and imaged with ^{89}Zr-5A10 24 hours post-injection after manipulation with a subcutaneous testosterone pellet or a daily oral gavage of vehicle or MDV3100 for 7 days. Arrows indicate the position of the tumor (T) and the murine liver (L). Right: region-of-interest analysis of the tumors from the PET study shows statistically significant changes in tumor-associated ^{89}Zr-5A10. $*P$, 0.01 compared with vehicle. $**P$, 0.05 compared with vehicle. Error bars represent the standard deviation from mean. Reprinted with permission from Ulmert, *et al.* Cancer Discovery 2012; ASAP.

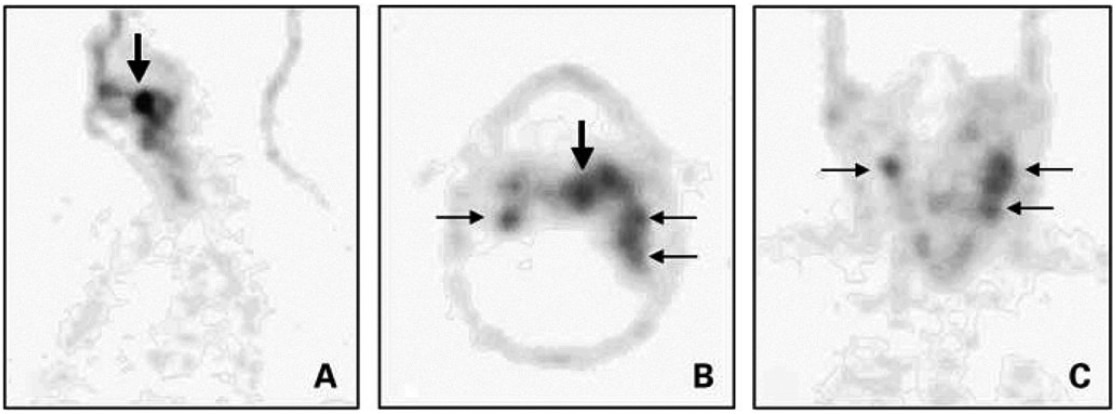

Figure 7.
ImmunoPET images with ^{89}Zr-cmAb U36 of head and neck cancer patient with a tumor in the left tonsil (large arrow) and lymph node metastases (small arrows) at the left (level II and III) and right (level II) side of the neck. Images were obtained 72 hours post-injection. A: sagittal image; B: axial image; and C: coronal image. Reprinted with permission from Borjesson, *et al.* Clinical Cancer Research 2006; 12: 2133-40.

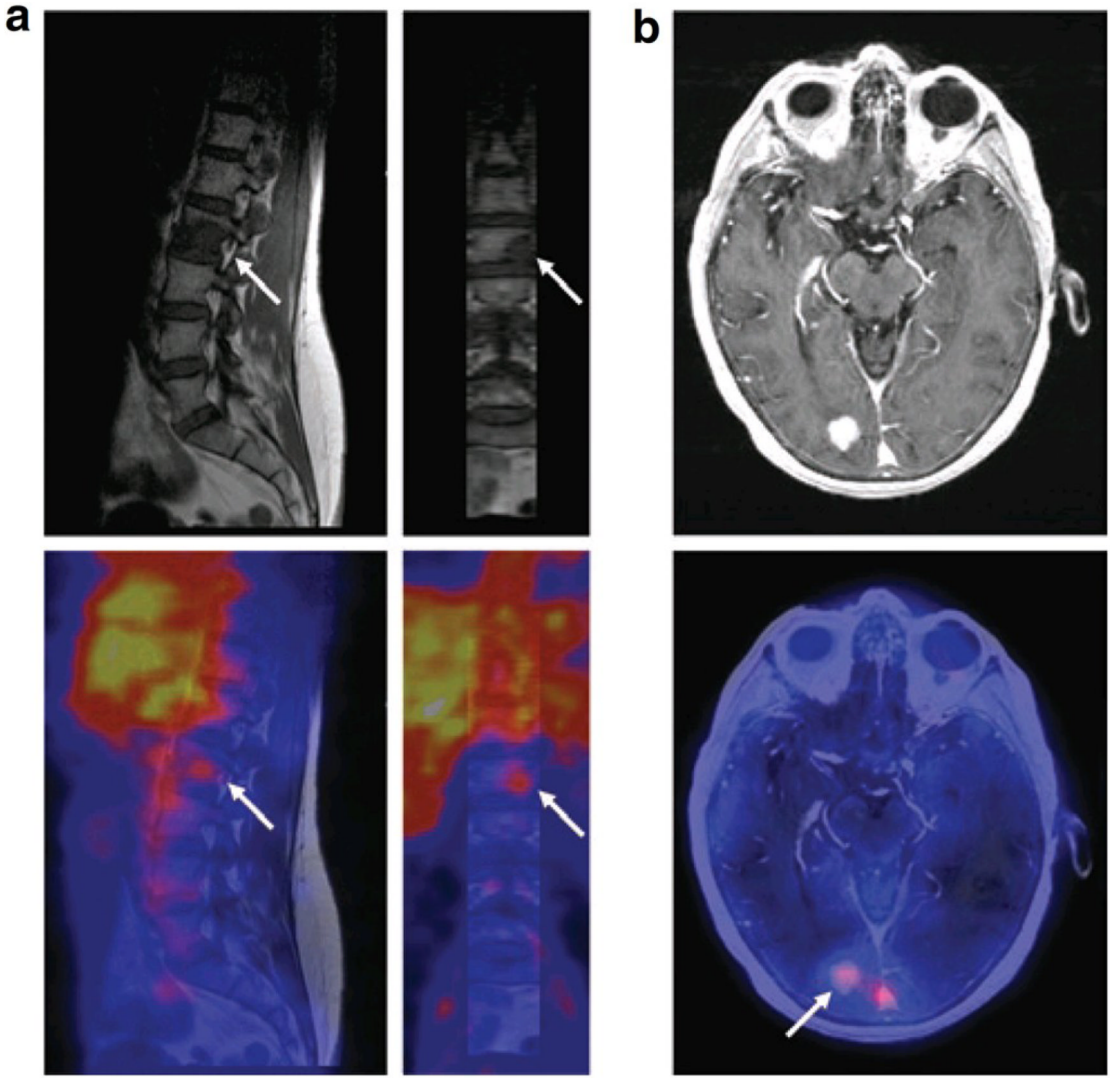

Figure 8.

Examples of fusion images from ^{89}Zr-Trasutuzmab PET and MRI scans. (a) In a vertebral metastasis seen on MRI but unapproachable for biopsy, HER2 status was revealed by ^{89}Zr-trastuzumab uptake on PET imaging. (b) Example of HER2-positive brain lesion undetected by conventional scans, revealed by ^{89}Zr-trastuzumab PET imaging, and subsequently confirmed by MRI. Arrows indicate lesions. Reprinted with permission from Dijkers, *et al.* J Nucl Med 2009; 50: 974-81.

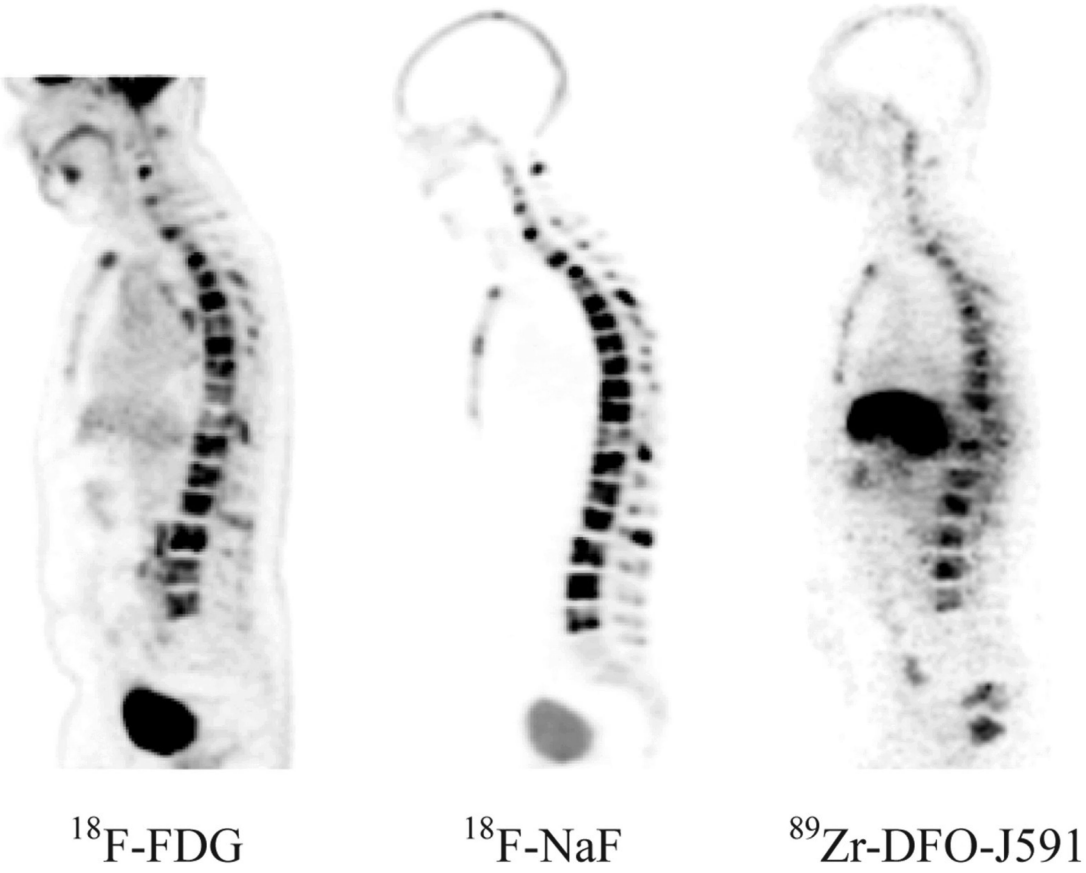

Figure 9.
^{18}F-FDG (13.2 mCi), ^{18}F-NaF (10.2 mCi), and ^{89}Zr-DFO-J591 (4.8 mCi) sagittal PET images of a 56 year-old male with castrate-resistant prostate cancer. Images courtesy of Drs. J. Carrasquillo, M. Morris, and S.M. Larson, MSKCC.

Table 1

Summary of pre-clinical imaging studies using ^{89}Zr-based imaging agents.

	Targeting Moiety	Target	Type of cancer	Conjugation Method	Reference
Antibodies	Cetuximab	EGFR	Multiple	*N*-suc-DFO	[70-73]
	Bevacizumab	VEGF	Head and neck squamous cell carcinoma; ovarian; breast	*N*-suc-DFO	[68, 71, 74, 75]
	Trastuzumab	HER2	Breast; ovarian	*N*-suc-DFO	[67, 75-77]
	J591	PSMA	Prostate	*N*-suc-DFO	[52] [78]
	cmAb U36	CD44v6	Head and neck squamous cell carcinoma	*N*-suc-DFO	[79, 80]
	5A10	fPSA	Prostate	*N*-suc-DFO	[65]
	cG250	MN/CA IX	Renal cell carcinoma	*N*-suc-DFO	[81]
	R1507	IGF-1R	Triple-negative breast	*N*-suc-DFO	[82]
	Fresolimumab	TGF-b	Multiple	*N*-suc-DFO	[83]
	DN30	Met	Gastric; head and neck squamous cell carcinoma	*N*-suc-DFO	[84]
	7E11	PSMA	Prostate	*N*-suc-DFO	[85]
	hRS7	EGP-1	Prostate	*N*-suc-DFO	[86]
	Panitumumab	HER1	Colorectal	DFO-Bz-NCS	[87]
	TRC105	CD105	Breast	DFO-Bz-NCS	[73]
	Anti-B220	B cells	Unspecified	DFO-Bz-NCS	[88]
	E48 and 323/A3	Unspecified surface antigens	Head and neck squamous cell carcinoma; ovarian	SATA/SMCC thioether	[66]
Antibody fragments	(aHGF) -Nanobodies	HGF	Glioma	DFO-Bz-NCS	[89]
	Ranibizumab (Fab)	VEGF-A isoforms	Ovarian	*N*-suc-DFO	[90]
	cG250-F(ab9)2	CAIX	Head and neck squamous cell carcinoma	*N*-suc-DFO	[91]
Peptides	c(RGDfK) with and w/o PEG	Integrin $\alpha v\beta 3$	Breast	DFO-Bz-NCS	[92]
Nanomaterials	Albumin	n/a	Prostate	*N*-suc-DFO	[93]
	resin microspheres and SIR-Spheres	n/a	Liver	n/a	[94]
	nanocolloidal albumin	n/a	Head and neck squamous cell carcinoma	DFO-Bz-NCS	[95]
	Dextran Nanoparticles	macrophages	Colon	DFO-Bz-NCS	[69]
	Single wall carbon nanotube	VE-cad based on attached antibody E4G10	Colon adenocarcinoma	*N*-suc-DFO	[96]